

## Article

# Unmanned Surface Vehicle Using a Leader–Follower Swarm Control Algorithm

Ji-Hyeong Lee <sup>1,2</sup>, Sang-Ki Jeong <sup>1</sup>, Dae-Hyeong Ji <sup>3</sup>, Hae-Yong Park <sup>1</sup>, Do-Young Kim <sup>1</sup>, Ki-Beom Choo <sup>4</sup> , Dong-Wook Jung <sup>4,5</sup>, Myung-Jun Kim <sup>6</sup>, Myoung-Hak Oh <sup>1</sup> and Hyeong-Sik Choi <sup>4,\*</sup> 

<sup>1</sup> Maritime ICT R&D Center, Korea Institute of Ocean Science and Technology, Busan 49111, Republic of Korea

<sup>2</sup> Ocean Science and Technology School, Korea Maritime and Ocean University, Busan 49112, Republic of Korea

<sup>3</sup> Marine Security and Safety Research Center, Korea Institute of Ocean Science and Technology, Busan 49111, Republic of Korea

<sup>4</sup> Department of Mechanical Engineering, Korea Maritime and Ocean University, Busan 49112, Republic of Korea

<sup>5</sup> Interdisciplinary Major of Ocean Renewable Energy Engineering, Korea Maritime and Ocean University, Busan 49112, Republic of Korea

<sup>6</sup> Maritime R&D Center, LIG Nex1 Co., Ltd., Seongnam-si 16911, Republic of Korea

\* Correspondence: hchoi@kmou.ac.kr; Tel.: +82-10-5581-2971

**Abstract:** To overcome the limitations of a single unmanned surface vehicle (USV), this study investigated the swarm control algorithms of USVs. Among various swarm control methods, a leader–follower swarm control method was selected and studied. The performance of the swarm algorithm proposed in this study was verified through an actual sea area test. A USV was designed and manufactured by dividing the power and communication parts. The power system was equipped with a coulometer to monitor the battery state in real time to protect the system through a switch linked to the coulometer in the case of abnormalities in the battery and to prevent accidents. In addition, a communication system was established to process the sensor data and camera image data of the USV in real time. Consequently, the desired swarm formation was achieved through the separately constructed swarm control algorithm. Before the actual sea area test, individual performance tests of each sensor were conducted. Finally, the performance of the swarm algorithm was verified by conducting a sea area test. The performance of the controllers was confirmed to be good, and the swarm formation was confirmed to be successful.

**Keywords:** unmanned surface vehicle; swarm control algorithm; leader–follower method; actual sea area test



**Citation:** Lee, J.-H.; Jeong, S.-K.; Ji, D.-H.; Park, H.-Y.; Kim, D.-Y.; Choo, K.-B.; Jung, D.-W.; Kim, M.-J.; Oh, M.-H.; Choi, H.-S. Unmanned Surface Vehicle Using a Leader–Follower Swarm Control Algorithm. *Appl. Sci.* **2023**, *13*, 3120. <https://doi.org/10.3390/app13053120>

Academic Editors: Wen-Hsiang Hsieh, Jia-Shing Sheu and Minvydas Ragulskis

Received: 1 February 2023

Revised: 19 February 2023

Accepted: 23 February 2023

Published: 28 February 2023



**Copyright:** © 2023 by the authors. Licensee MDPI, Basel, Switzerland. This article is an open access article distributed under the terms and conditions of the Creative Commons Attribution (CC BY) license (<https://creativecommons.org/licenses/by/4.0/>).

## 1. Introduction

The marine environment occupies about 71% of the Earth's surface and has various resources such as oil, natural gas, rare earth elements, and aquatic resources [1]. As the importance of securing such resources has emerged, various countries are developing offshore platforms for seabed surveys and maintenance of submarine structures such as gas pipelines and submarine cables [2,3]. Until now, most of these tasks, such as seafloor surveying and submarine structure maintenance and repair, have been carried out in a way that requires divers to dive directly to and work at the site [4]. However, even if a human wears professional equipment, continuously working for more than an hour at a depth of 30 m or more is difficult. Further, because professional skills are required, there is a disadvantage of high cost if a human is working in deep marine locations. Therefore, several studies on the investigation of the seabed and the inspection of damaged areas of subsea structures using acoustic image sensors such as sonar and multi-beam in unmanned surface vehicles (USVs) are in progress [5,6].

The multi-object USV system has a wider range of applications than the single-unit USV system for missions such as exploration and environmental investigation. In addition,

the use of several objects simultaneously provides various advantages such as improved mission performance, increased efficiency, and energy saving. Thus, studies related to the multi-object USV system to which the swarm control algorithm is applied are receiving a lot of attention [7–10].

There are three major swarm control methods: behavior-based swarm control, virtual structure swarm control, and leader–follower swarm control [11]. Although each swarm control method has different advantages and disadvantages, the double leader–follower swarm control is easy to understand and express mathematically. Further, theoretically, the number of followers can be increased without limit. Thus, a multi-object USV system is advantageous to construct [12–14]. Communication methods used in leader–follower swarm control include centralization and decentralization methods. In the centralization method, the implementation of the swarm control algorithm is easier than in the decentralization method. However, in the decentralization method, information sharing time is shorter than in the centralization method and it is difficult to build infrastructure such as server rooms and use them in environments where it is impossible to fix the location of the land operation console. Therefore, the decentralization method is more suitable for the marine mission environment [8].

In this study, a multi-object USV system was constructed using a leader–follower swarm control algorithm using a distributed method that allows the movement of a land operation console according to the characteristics of the marine environment. To this end, a land operation console and an operation program were developed. In addition, to verify the performance of the leader–follower swarm control algorithm proposed herein, a USV capable of three-degree-of-freedom (DOF) motion was designed and developed. To enable smooth route control in a marine environment with many disturbances, a controller was designed considering cross-track error (CTE), and its performance was verified. In addition, a sensor verification experiment was conducted to confirm the reliability of the sensor used in the study. Finally, the designed leader–follower swarm control algorithm was installed in the USV, and its performance was verified by experimenting in an actual sea area.

However, despite the importance of developing such a multi-object system, the level of development of multi-object systems is low [15]. Therefore, in this study, USVs equipped with a leader–follower swarm control algorithm were developed, and their performance was verified.

## 2. USV Modeling and Leader–Follower Swarm Formation

### 2.1. Modeling of the USV

Figure 1 and Table 1 show the USV coordinate system and the notation used by the Society of Naval Architects and Marine Engineers.

The rigid body dynamics modeling of the USV was designed based on the Newton–Euler equation and vectorial matrix dynamics. Roll, pitch, and heave motions were excluded from modeling because the USV is a three-DOF platform that performs translational motion along the X and Y axes and rotational motion around the Z axis. According to [16], the rigid body dynamic equation of the USV can be expressed in the form of Equation (1).

$$\dot{M}_{RB}v + C_{RB}(v)v = \tau_{RB} \quad (1)$$

Here,  $M_{RB}$  is the mass and inertia matrix of the USV,  $C_{RB}(v)$  is the Coriolis force and centripetal force matrix, and  $\tau_{RB}$  is the external force caused by the USV thruster. However, a method such as Equation (1) is an expression of an ideal situation. To represent it in a realistic expression, the definition of fluid force should be included in the rigid body dynamic equation. The rigid body dynamic equations including fluid force are expressed as Equation (2).

$$\begin{aligned}
 (m - X_{\dot{u}})\dot{u} - u_r + (Y_{\dot{v}}v_r r + Y_{\dot{r}}r - mX_G r) - (X_u + X_{u|u}|u|)u &= \tau_X \\
 (m - y_{\dot{v}})\dot{v} + (mX_G - Y_{\dot{r}})\dot{r} + u_r - X_{\dot{u}}u_r r - (Y_v + Y_{v|v}|v|)v - (Y_r + Y_{r|r}|r|)r &= \tau_Y \\
 (mX_G - N_{\dot{v}})\dot{v} + (I_Z - N_{\dot{r}})\dot{r} - (Y_{\dot{v}}v_r r - Y_{\dot{r}}r + mX_G r)u + X_{\dot{u}}u_r v - (N_v + N_{v|v}|v|)v \\
 - (N_r + N_{r|r}|r|)r &= \tau_N
 \end{aligned} \tag{2}$$

Here,  $\tau$  is the thrust of the USV thruster. Detailed definitions of the variables and conditions for Equation (2) can be found in [17–19].

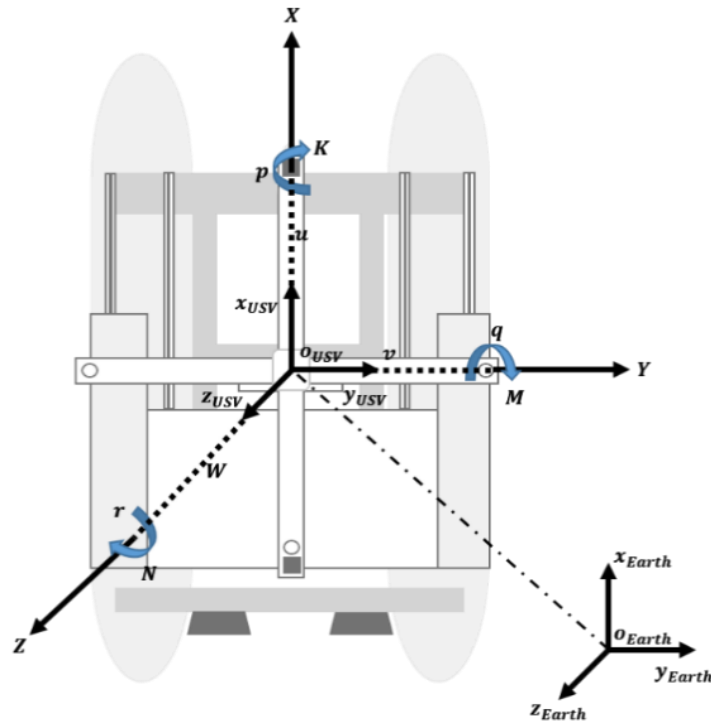


Figure 1. Coordinates of the unmanned surface vehicle.

Table 1. Notation of the Society of Naval Architects and Marine Engineers for the unmanned surface vehicle.

	Force and Moments	Linear and Angular Velocity	Position and Euler Angle
Motion in the X direction (surge)	X	$u$	$x$
Motion in the Y direction (sway)	Y	$v$	$y$
Motion in the Z direction (heave)	Z	$w$	$z$
Rotation about the X axis (roll)	K	$p$	$\phi$
Rotation about the Y axis (pitch)	M	$q$	$\theta$
Rotation about the Z axis (yaw)	N	$r$	$\psi$

### 2.2. Modeling of the Leader–Follower Swarm Formation

The USV uses the method of moving two thrusters independently. At this time, assuming that the thruster does not cause slip or cavitation in water, the USV has nonholonomic constraints such as Equations (3) and (4).

$$\dot{X}_c \sin \theta_c - \dot{Y}_c \cos \theta_c = 0 \tag{3}$$

$$\begin{bmatrix} \dot{X}_c(t) \\ \dot{Y}_c(t) \\ \dot{\theta}_c(t) \end{bmatrix} = \begin{bmatrix} \cos(\theta_c(t)) & 0 \\ \sin(\theta_c(t)) & 0 \\ 0 & 1 \end{bmatrix} \begin{bmatrix} v_c(t) \\ w_c(t) \end{bmatrix} \tag{4}$$

Here,  $X_c(t)$  and  $Y_c(t)$  denote the X and Y axes of the USV, and  $\theta_c(t)$  denotes its direction angle. The  $v_c(t)$  and  $w_c(t)$  denote the linear and angular velocities of the USV, and  $v_c$  and  $w_c$  denote the control input of the USV.

Figure 2 shows a kinematic model of a leader–follower swarm with nonholonomic constraints.

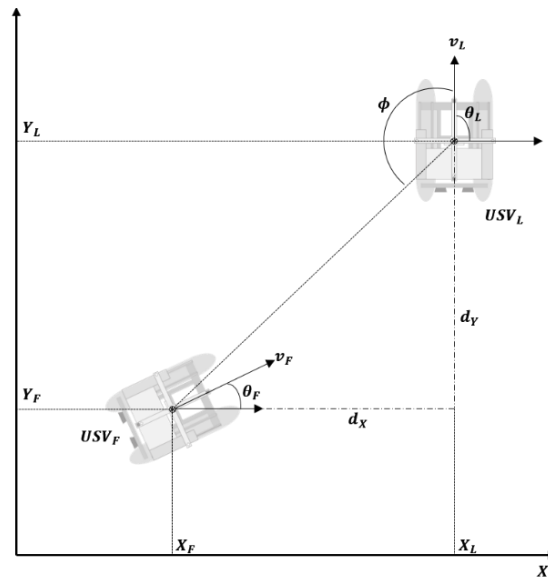


Figure 2. Kinematic model of the leader–follower unmanned surface vehicles.

The leader USV is expressed using the subscript L, and the follower USV is expressed using the subscript F. The variables  $X_L$  and  $Y_L$  represent the current position of the leader USV, and  $\theta_L$  is its direction angle. Similarly,  $X_F$  and  $Y_F$  denote the current position of the follower USV, and  $\theta_F$  denotes its direction angle. Additionally,  $v_L$  and  $v_F$  indicate the straight-line speed of each USV. The distance coordinates  $d_X$  and  $d_Y$  between the leader USV and the follower USV are expressed in the Cartesian coordinate system as Equation (5)

$$\begin{aligned} d_X(t) &= X_L(t) - X_F(t) = -d(t) \cos(\phi(t) + \theta_L(t)) \\ d_Y(t) &= Y_L(t) - Y_F(t) = -d(t) \sin(\phi(t) + \theta_L(t)) \end{aligned} \tag{5}$$

Here, the current position of the follower USV is expressed as a relational expression with the leader USV as Equation (6).

$$\begin{aligned} X_F(t) &= X_L(t) + d \cos(\phi(t) + \theta_L(t)) \\ Y_F(t) &= Y_L(t) + d \sin(\phi(t) + \theta_L(t)) \end{aligned} \tag{6}$$

Here, the distance  $d^2 = d_X^2 + d_Y^2$  between the leader USV and the follower USV is the azimuth  $\phi(t) = \tan^{-1}\left(\frac{d_Y}{d_X}\right) - \theta_L(t) + \pi$  between the leader USV and the follower USV.

The role of the follower USV is to take a position with a specific distance and a specific angle designated by the land operation console relative to the position of the leader USV and to follow the trajectory. Equation (7) express the formation position of the USV following the leader USV.

$$\begin{aligned} X_F^d(t) &= X_L(t) + d_{ref} \cos(\phi_{ref} + \theta_L(t)) \\ Y_F^d(t) &= Y_L(t) + d_{ref} \sin(\phi_{ref} + \theta_L(t)) \\ \theta_F^d(t) &= \theta_L(t) \end{aligned} \tag{7}$$

Here,  $X_F^d(t)$  and  $Y_F^d(t)$  indicate the position to be attained by the follower USV, and  $d_{ref}$  is the distance between a trajectory to be followed by the leader USV and the follower USV. In this case, the distance cannot be negative, so it is always expressed as a positive number. The  $\phi_{ref}$  represents the angle that the follower USV aims to maintain from the leader USV, and this value is expressed as a constant, not a function. By differentiating Equation (7), the coordinate change in the follower USV can be obtained Equation (8).

$$\begin{aligned} \dot{X}_F^d(t) &= v_L(t) \cos(\theta_L(t)) - d_{ref} \sin(\phi_{ref} + \theta_L(t)) \omega_L(t) \\ \dot{Y}_F^d(t) &= v_L(t) \sin(\theta_L(t)) + d_{ref} \cos(\phi_{ref} + \theta_L(t)) \omega_L(t) \end{aligned} \tag{8}$$

The definitions of the variables and conditions related to these equations can be found in [20].

### 3. Control Algorithm of the USV

#### 3.1. CTE Compensation Algorithm

CTE represents the vertical distance error between the target path of the platform and the actual movement path caused by various disturbances such as waves and wind. Figure 3 shows a schematic of CTE.

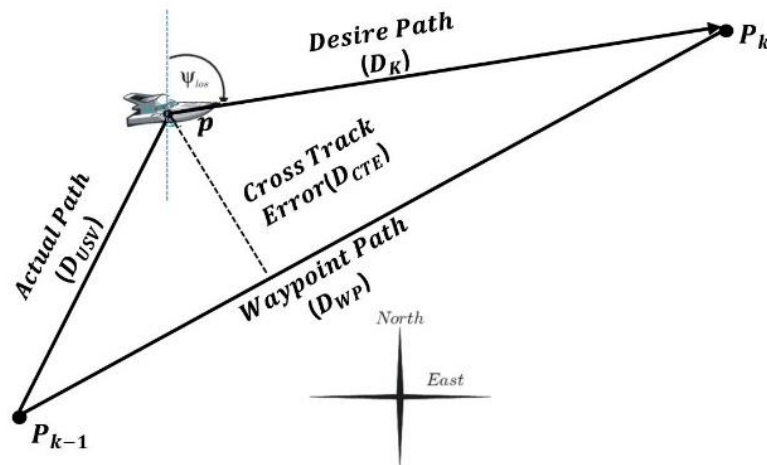


Figure 3. Schematic of cross-track error.

This CTE can be calculated using Heron’s formula, which uses  $S$ , half the value of the sum of the three paths shown in Figure 3: the straight path  $D_K$ , the path  $D_{USV}$  that the USV had previously targeted, and the waypoint path  $D_{WP}$  that the USV had to travel to reach the target point. The CTE value calculated through Heron’s formula is expressed as Equation (9).

$$D_{CTE} = \frac{2\sqrt{S(S - D_{USV})(S - D_K)(S - D_{WP})}}{D_{WP}} \tag{9}$$

When CTE occurs during operation, the result value of image sonar sensors such as side scan sonar (SSS) and multi-beam is abnormal, or it consumes more energy to reach the target point. Thus, it has a negative effect on energy efficiency.

In this study, the automatic navigation function of the USV was improved by including a compensation algorithm that compensated for CTE in the operation-related control function of the USV. Figure 4 shows a schematic representation of the CTE compensation algorithm.

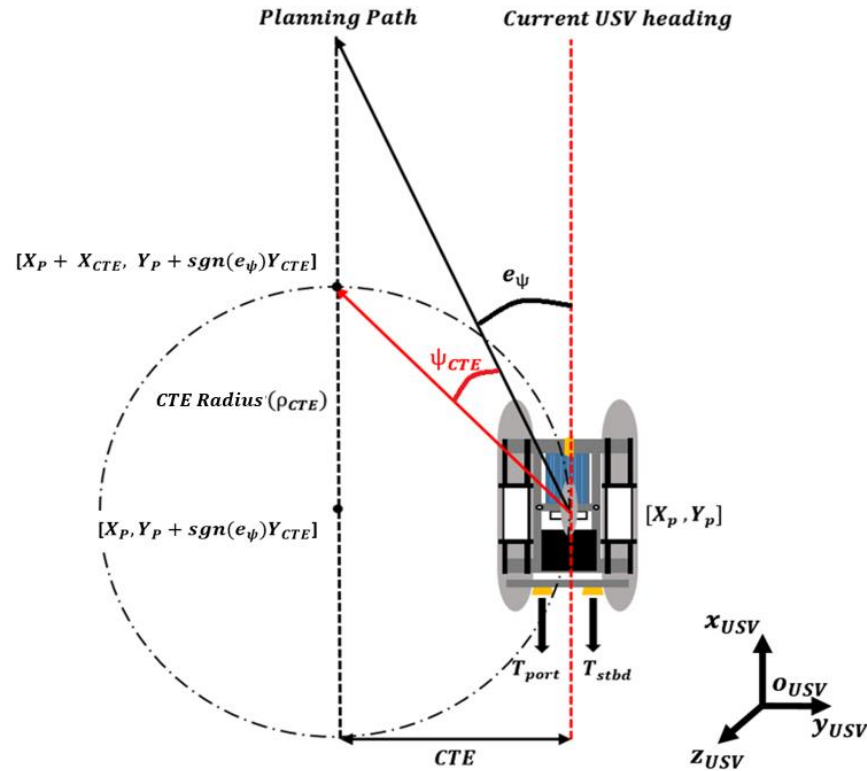


Figure 4. Schematic of the cross-track-error compensation algorithm.

The CTE compensation algorithm is used to improve the forward control performance of the USV. To reduce the CTE occurring during forward movement, the coordinates  $[X_p, Y_p + \text{sgn}(e_\psi)Y_{CTE}]$  are newly created from the center point  $[X_p, Y_p]$  of the USV to the Y axis moved by  $Y_{CTE}$ .

After that, an imaginary circle  $\rho_{CTE}$  with the newly created point as the center point is drawn, and a new target direction angle  $\psi_{CTE}$  is obtained that targets the bow direction contact point  $[X_p + X_{CTE}, Y_p + \text{sgn}(e_\psi)Y_{CTE}]$  between the circle and the target path.

Through the difference between  $e_\psi$ , which is the target direction angle of the existing USV, and the new target direction angle  $\psi_{CTE}$ , the error value  $E_{CTE}$  is used as a new error value for the control. Equation (10) are mathematical expressions of the control algorithm to which CTE compensation is applied [17].

$$E_\psi = e_\psi - \psi_{CTE} \tag{10}$$

$$T_{CTE} = K_{P\psi}E_\psi + K_{I\psi} \int E_\psi + K_{D\psi}\dot{E}_\psi$$

Here,  $T_{CTE}$  represents the output value of the controller to which CTE compensation is applied. The controller outputs the driving force of the port-side and starboard-side thrusters according to the sign of the  $e_\psi$  value of the USV. Figure 5 shows a block diagram of the controller to which the CTE compensation algorithm is applied.

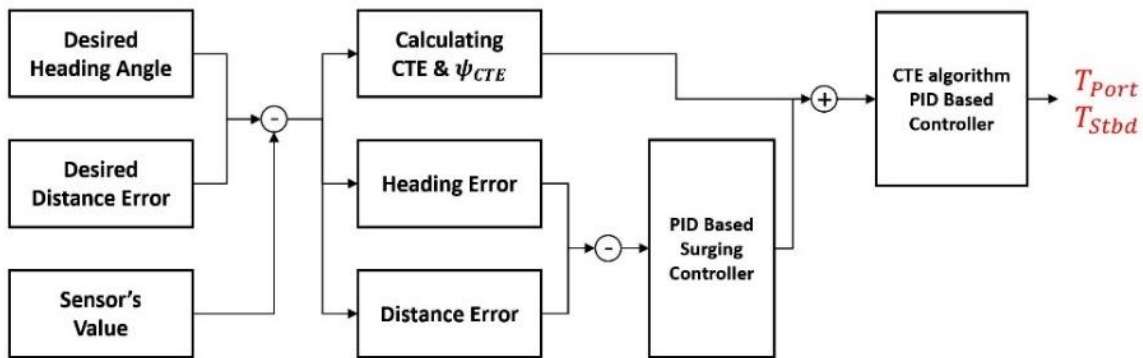


Figure 5. Block diagram of the cross-track error compensation algorithm.

### 3.2. Swarm Control Algorithm

To maintain the formation of the platoon in swarm control using the leader–follower swarm control method, a virtual point is created at a certain distance and a certain angle from the leader USV. The follower USV must follow the point. The virtual point makes it possible to maintain the desired group formation because a certain distance and a certain angle can be maintained regardless of the actual leader USV’s movement. Figure 6 shows the behavior of the follower USV following the virtual point in the Cartesian coordinate system.

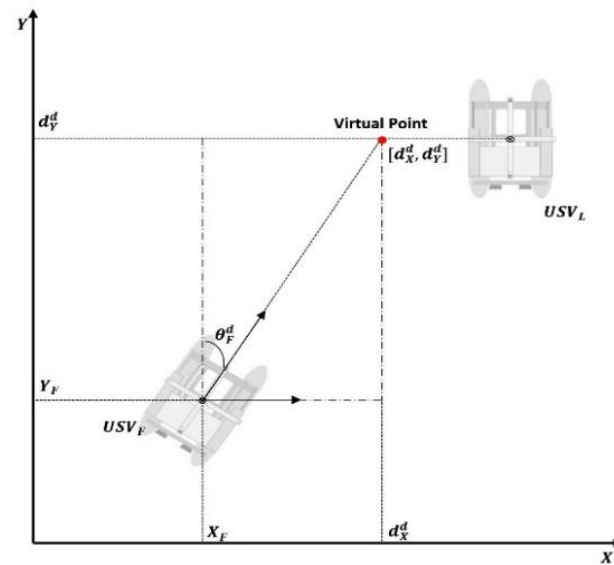


Figure 6. Schematic of the follower unmanned surface vehicle and virtual point.

According to [21,22], the error between the point created virtually and the trajectory followed by the follower USV can be expressed as Equation (11).

$$\begin{aligned}
 \begin{bmatrix} e_{X2}(t) \\ e_{Y2}(t) \\ e_{\theta2}(t) \end{bmatrix} &= \begin{bmatrix} \cos(\theta_F(t)) & \sin(\theta_F(t)) & 0 \\ -\sin(\theta_F(t)) & \cos(\theta_F(t)) & 0 \\ 0 & 0 & 1 \end{bmatrix} \begin{bmatrix} d_X^d(t) - d_X(t) \\ d_Y^d(t) - d_Y(t) \\ \theta_F^d(t) - \theta_F(t) \end{bmatrix} \\
 &= \begin{bmatrix} d_X^d(t) \cos(\phi_{ref} + e_{\theta2}(t)) - d_X(t) \cos(\phi(t) + e_{\theta2}(t)) \\ d_Y^d(t) \sin(\phi_{ref} + e_{\theta2}(t)) - d_Y(t) \sin(\phi(t) + e_{\theta2}(t)) \\ \theta_L(t) - \theta_F(t) \end{bmatrix} \tag{11}
 \end{aligned}$$

Here,  $[X_F(t), Y_F(t), \theta_F(t)]$  is the position and direction angle of the follower USV;  $[d_X^d(t), d_Y^d(t)]$  is the position of the virtual point; and  $\theta_F^d(t)$  is the azimuth to the follower point. As  $\theta_F^d(t)$  is the same as the direction angle  $\theta_L(t)$  of the leader USV, it can be expressed

differently. Substituting Equations (5) and (6) into Equation (11), the error between the virtual point and the trajectory followed by the follower USV can be obtained Equation (12).

$$\begin{aligned}
 e_{X2}(t) &= (X_L(t) - X_F(t)) \cos(\theta_F(t)) + (Y_L(t) - Y_F(t)) \sin(\theta_F(t)) + d_{ref} \cos(\phi_{ref} + \theta_L(t) - \theta_F(t)) \\
 e_{Y2}(t) &= -(X_L(t) - X_F(t)) \sin(\theta_F(t)) + (Y_L(t) - Y_F(t)) \cos(\theta_F(t)) + d_{ref} \sin(\phi_{ref} + \theta_L(t) - \theta_F(t)) \\
 e_{\theta2}(t) &= \theta_L(t) - \theta_F(t)
 \end{aligned}
 \tag{12}$$

Here, by using the calculated value, the distance error  $d_{e2} = \sqrt{e_{X2}(t)^2 + e_{Y2}(t)^2}$  between the virtual point and the USV can be obtained. The controller of the follower USV with the distance and azimuth errors as control inputs is expressed as Equation (13).

$$\begin{aligned}
 T_{\theta2} &= K_{P_{\theta2}} e_{\theta2} + K_{I_{\theta2}} \int e_{\theta2} + K_{D_{\theta2}} \dot{e}_{\theta2} \\
 T_{d_{e2}} &= K_{P_{d_{e2}}} e_{d_{e2}} + K_{I_{d_{e2}}} \int e_{d_{e2}} + K_{D_{d_{e2}}} \dot{e}_{d_{e2}}
 \end{aligned}
 \tag{13}$$

Here,  $T_{\theta2}$  and  $T_{d_{e2}}$  denote the direction and distance output from the controller, respectively, and  $e_{\theta2}$  and  $e_{d_{e2}}$  denote the azimuth and distance error between the virtual point and the current position of the follower USV.

For effectively maintaining the leader–follower swarm formation, the control algorithm should consider rotation, as shown in Figure 7.

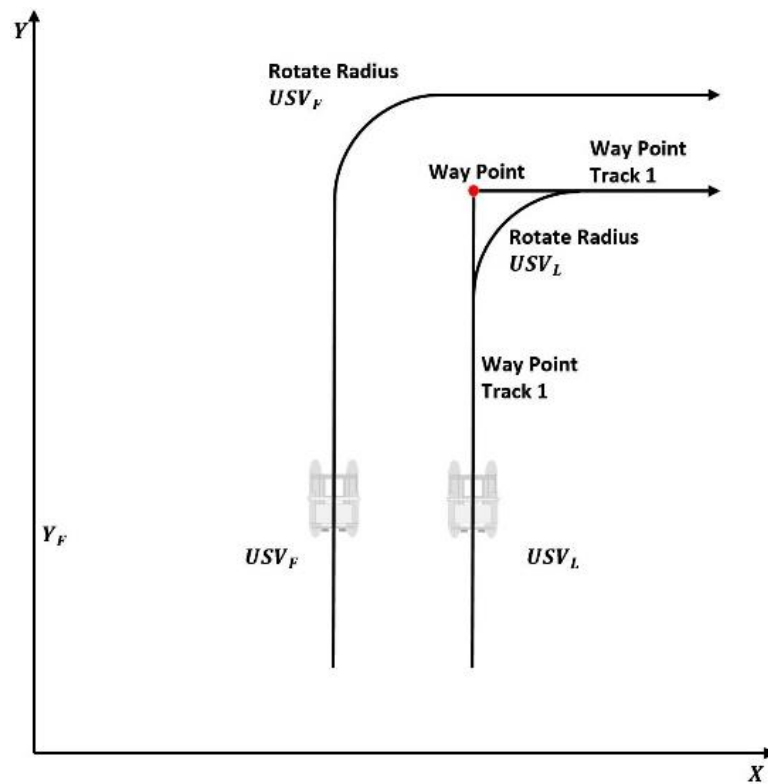
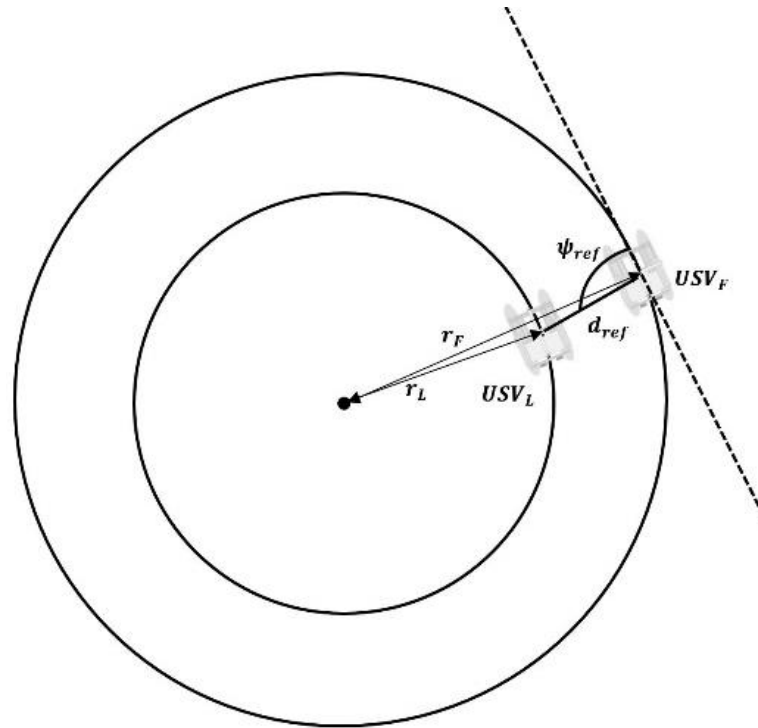


Figure 7. Rotation of the leader–follower control.

Considering the rotation situation, for the design of a controller that can maintain effective formation, the exact formation control technique proposed in [23] is used. Equation (14) expresses the exact formation control.

$$v_F = v_L \frac{\cos(\beta_{LF} - \psi_{ref})}{\cos(\psi_{ref})}
 \tag{14}$$

Here,  $v_L$  and  $v_F$  represent the linear velocity of the leader and follower USVs, respectively;  $\beta_{LF}$  represents the difference between the azimuths of the leader and follower USVs; and  $\psi_{ref}$  represents the target azimuth of the leader USV. Assuming the formation that the follower USV is on the right side concerning the leader USV, the relationship between the turning radius of each USV and the formation control can be expressed in detail, as shown in Figure 8.



**Figure 8.** Relationship of the rotation radius and formation control.

As shown in Figure 7, to maintain the crossbar formation, the follower USV must move along a circle with radius  $r_F$ . Furthermore, as the movement distance of the follower USV is larger, the movement speed of the follower USV should exceed that of the leader USV. Equation (15) shows the relationship between the turning radii of the leader and follower USVs.

$$r_L = (d_{ref})^2 + (r_F)^2 - 2d_{ref}r_F \cos\left(\frac{\pi}{2} - \psi_{ref}\right) \tag{15}$$

Here,  $d_{ref}$  is a straight line connecting any point within the turning radius of the leader USV and any other point within the turning radius of the follower USV. The  $\psi_{ref}$  represents the angle between  $d_{ref}$  and the turning radius of the follower USV. After Equation (15) is arranged for  $r_F$  and solved using the quadratic formula, it is expressed as Equation (16).

$$r_F = d_{ref} \sin(\psi_{ref}) \pm \sqrt{d_{ref}^2 (\sin(\psi_{ref}))^2 + r_L^2 - d_{ref}^2} \tag{16}$$

Both negative and positive values of the turning radius of the follower USV are shown in Figure 9.

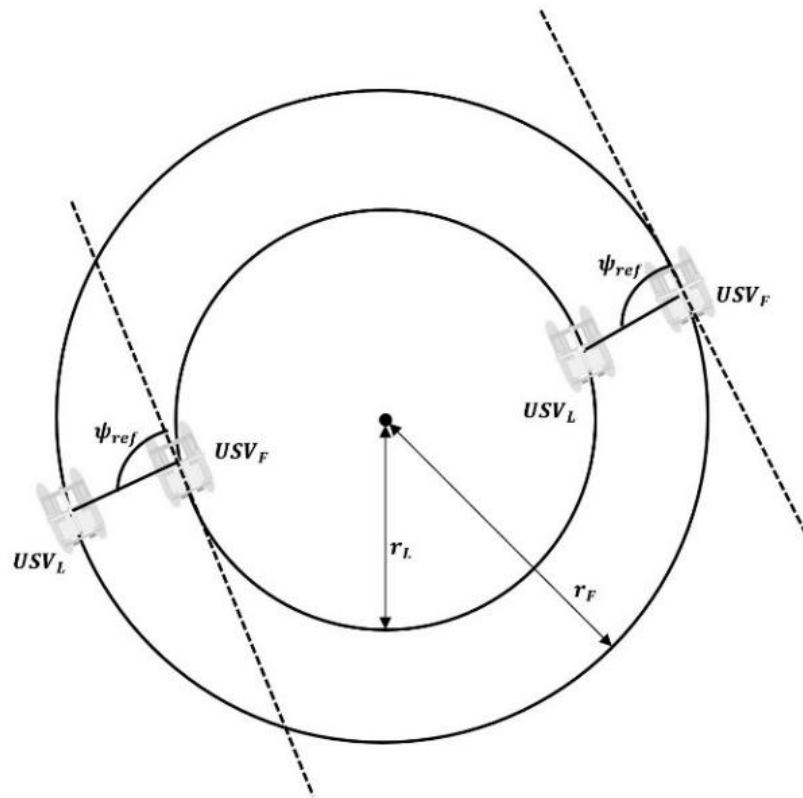


**Figure 9.** Two cases of the follower USV rotation radius.

The two roots are divided according to the formation made by the leader USV and the follower USV. Therefore, the rotation radius  $r_F$  of the follower USV, considering whether the position of the follower USV is located on the left side or the right side of the leader USV, is arranged as shown in Equation (17).

$$r_F = d_{ref} \sin(\psi_{ref}) \pm \alpha \sqrt{d_{ref}^2 (\sin(\psi_{ref}))^2 + r_L^2 - d_{ref}^2}$$

$$\alpha = 1 \text{ if } r_L \geq r_F$$

$$\alpha = -1 \text{ if } r_L \leq r_F$$
(17)

Here,  $r_L = v_L/w_L$  and  $r_F = v_F/w_F$  are the turning radii of the leader and follower USVs, and  $w_L = w_F$  to maintain formation. The speed adjustment of the follower USV is expressed as Equation (18).

$$v_F = v_L + (r_F - r_L)w_L$$
(18)

Therefore, if the speed adjustment derived from Equation (18) is used to obtain the error value of the follower USV controller, formation control between the leader USV and the follower USV is possible even upon rotation. Detailed definitions of the variables and conditions of the rotation algorithm used in this study can be found in [24].

#### 4. System Structure of the USV

In this study, to apply the leader–follower swarm control algorithm, two USVs (leader and follower) with the same structure equipped with two thrusters were manufactured. Figure 10 shows the manufactured USV, and Table 2 lists the USV specifications.

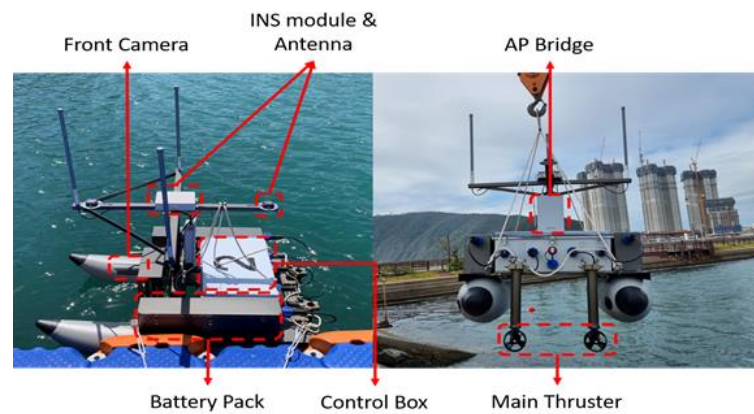


Figure 10. Leader and follower unmanned surface vehicles manufactured in this study.

Table 2. Specifications of the leader and follower unmanned surface vehicles.

Size (L × W × H)	1500 × 920 × 920 (mm)
Weight	60 (kgf)
Navigation sensor	Marineinnotec K-STAR
Battery	25.9 V, 75 Ah
Camera	Hanwha QNO-6012R
Main controller	MSI cubi 5 10M
AP bridge	GT-Wave 860S
Thruster	CiLab T80-60

#### 4.1. Power System of the USV

The power system of the USV consists of a battery, a coulometer, an indicator, a DC/DC converter, etc. The battery is the most important component that determines the USV operating time. Therefore, in this study, the battery with the most suitable capacity for the USV was selected according to the battery-energy amount calculation formula (Equation (19)).

$$W_h = \frac{(W_{USV} \times L_f \times H \times O_P)}{(B_a \times S_f)} \tag{19}$$

Here,  $w_h$  is the total uptime of the platform,  $w_{USV}$  is the total power consumption of the entire system,  $L_f$  is the average load factor of the system,  $H$  is the operating time with one charge,  $O_P$  is the operating rate of the system,  $B_a$  is the usable capacity compared to the total capacity of the battery, and  $S_f$  is the safety factor. Information on the related equations and variables can be found in [25].

In this study, the total power consumption of the entire system was the sum of the thruster and CPU capacity, and the average load ratio and operation rate were limited to 40%. The usable capacity compared to the total capacity of the battery was set to 80%, the value recommended by the battery manufacturer, and the battery was selected with a safety factor of 1.5.

Figure 11 shows the configuration diagram of the developed USV power system. Two Li-ion type batteries with a wattage of 25.9 V and 75 Ah were connected in parallel. The Li-ion type battery is used in this study because it is lighter in weight to volume and has high energy density compared to Li-polymer or LiFePo<sub>4</sub> batteries. However, Li-ion batteries have a fatal flaw of the memory phenomenon and a high risk of explosion. Therefore, in this study, the circuit of the power system was configured in such a way that a coulometer indicator and an electronic switch were installed to monitor the voltage input/output to the battery in real time and to cut off the power in the case of a problem. In addition, a battery management system (BMS) was additionally installed in the battery to handle the memory phenomenon, overcharge, and overdischarge.

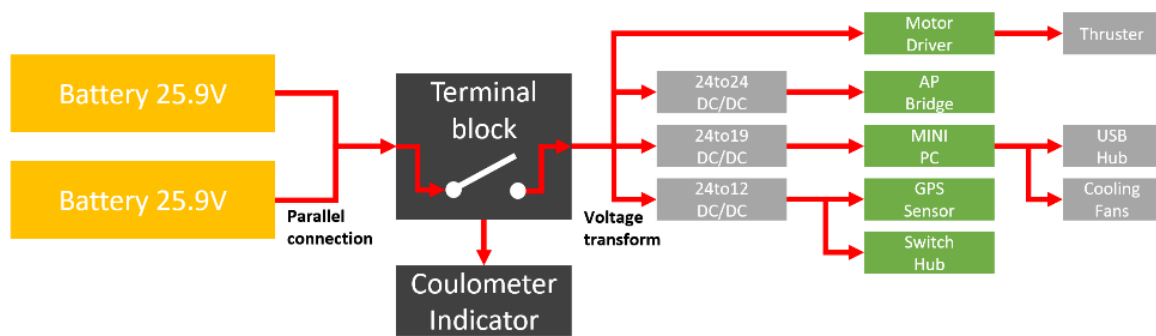


Figure 11. Configuration diagram of the power system.

#### 4.2. Communication System of the USV

Communication between the land operation console and each USV is performed through the access point (AP) bridge. Commands transmitted from the land operation console are transmitted to the receiving antennas of each USV through the AP bridge and are classified by the switch hub installed inside and delivered to each required place. In addition, the communication system was designed so that information such as position, direction angle, and operation speed could be shared between the leader and the follower. Figure 12 is a block diagram showing the communication system between the land operation console and the leader and follower USVs.

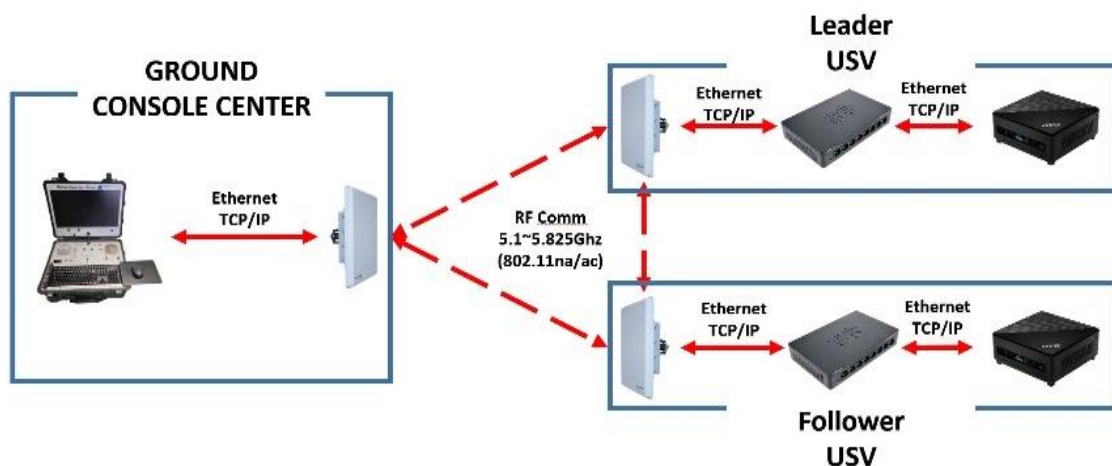


Figure 12. Configuration diagram of the communication system.

#### 4.3. Configuration of the Operating System

##### 4.3.1. Design of the Ground Operation Console

The land operation console is a device that transmits mission commands to each USV. It is waterproof and has a wheeled carrier for marine exploration missions where the installation location often changes each time a mission is performed. An AC/DC converter, commercial PC parts, a USB serial expansion port, and an Ethernet expansion port for supplying power to communication equipment are installed inside the waterproof case. Considering that it is mainly used in a salty environment, a bracket, jig, storage space, and top plate for fixing internal parts were manufactured using an aluminum material that does not easily corrode. The operating console's operating system (OS) is a user-friendly Windows and is equipped with a graphical user interface (GUI) program and a remote access program that can be directly connected to the USV. Figure 13 shows the internal and external configuration of the land operation console manufactured in this study.

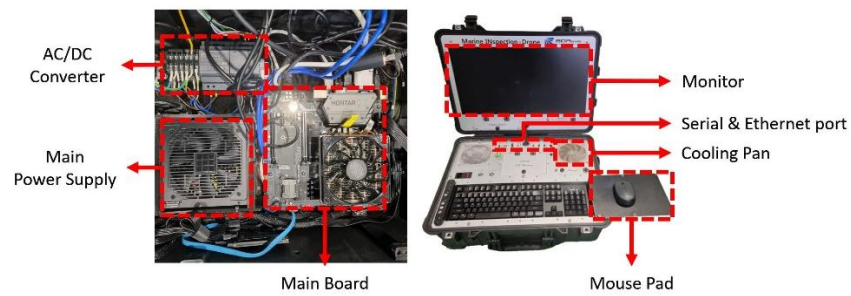


Figure 13. Configuration of the ground operation console.

### 4.3.2. Design of the GUI Monitoring Program

The monitoring program was created for collecting data such as cameras, posture, direction angle, and cruising speed of the leader and follower USVs, and transmitting control commands to each USV. It was created using Visual Studio C#, which allows users to easily check data, check the platform behavior, and control the USV. The monitoring program displays the information of the leader and follower USVs, and by linking with Google Maps, one can check the information of the sea area where the actual USV is performing its mission and the direction each USV is looking in detail. For route control, there is no need to check the point coordinates of the point. If one clicks on the desired area, the route control proceeds to the point. Various functions such as emergency stop function, camera image check, and data storage in the case of a problem are implemented. Furthermore, it includes a sensor state indicating function that determines the reliability of information coming from the current USV and informs the user using color. Figure 14 shows the composition of the prepared monitoring program.



Figure 14. Configuration of the console monitoring program.

## 5. Performance Test and Actual Sea Area Test of the Swarm USV

### 5.1. Sensor Performance Test

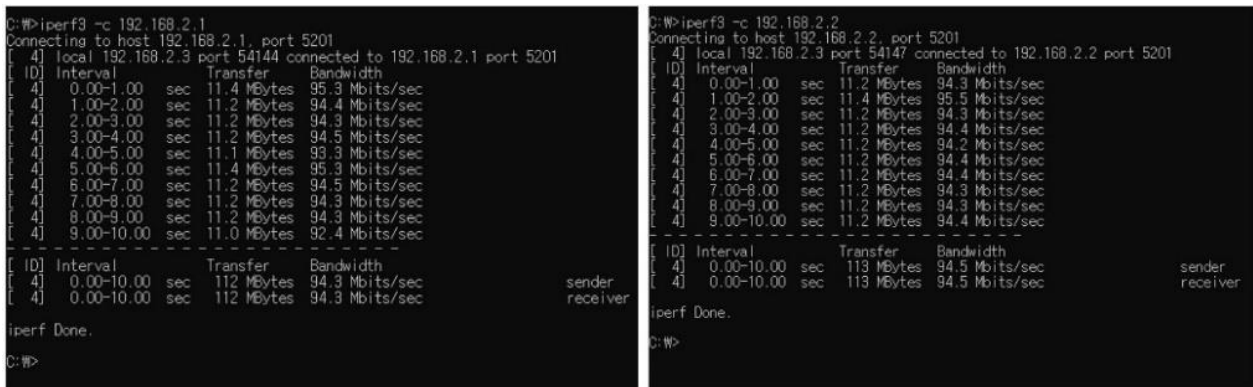
In this study, the data reliability was verified through a performance test of the sensors installed in each USV before the actual sea area test.

#### 5.1.1. Communication Speed Test

In the leader–follower swarm control, communication between the land operation console and the leader and follower USVs should proceed smoothly. The communication method adopted in this study, the decentralization method, acquires and controls each data point. Thus, communication between the land operation console and the leader and follower USVs is not smooth. Consequently, the swarm formation is difficult to maintain, and due to the delay time, the checkpoint can be incorrectly calculated at a place other than the target route. Therefore, a performance test of the communication equipment installed in each USV was conducted in the following two cases:

1. Communication speed test between the land operation console and each USV; and
2. Communication speed test between the leader and follower USVs.

The communication speed test between the land operation console and the USV was conducted to verify whether the real-time data coming from the sensors mounted on the USV were secured. Transmitting equipment and receiving equipment were placed at a distance of about 200 m, and the communication speed was measured using a communication speed measurement program. The communication speed measurement program used was Iperf3. The experimental results are shown in Figure 15.



Ground <-> Leader USV

Ground <-> Follower USV

Figure 15. The test result of communication speed test 1.

The communication speed measurement result was 94.3 Mbps between the land operation console and the leader USV, and 94.5 Mbps between the land operation console and the follower USV. The transmission bandwidth of the camera most affected by the communication speed among the sensors installed in the USV was 80 Mbps or more.

Figure 16 shows the communication speed test result between the leader USV and the follower USV.

```

C:\#>iperf3 -s
-----
Server listening on 5201
-----
Accepted connection from 192.168.2.1, port 59705
[ 5] local 192.168.2.2 port 5201 connected to 192.168.2.1 port 59706
[ ID] Interval      Transfer    Bandwidth
[ 5] 0.00-1.01    sec 12.0 MBytes 100 Mbits/sec
[ 5] 1.01-2.00    sec 13.1 MBytes 111 Mbits/sec
[ 5] 2.00-3.00    sec 12.9 MBytes 108 Mbits/sec
[ 5] 3.00-4.00    sec 13.4 MBytes 113 Mbits/sec
[ 5] 4.00-5.00    sec 12.1 MBytes 102 Mbits/sec
[ 5] 5.00-6.00    sec 13.1 MBytes 110 Mbits/sec
[ 5] 6.00-7.00    sec 12.9 MBytes 108 Mbits/sec
[ 5] 7.00-8.00    sec 12.5 MBytes 105 Mbits/sec
[ 5] 8.00-9.00    sec 12.9 MBytes 108 Mbits/sec
[ 5] 9.00-10.00   sec 12.8 MBytes 107 Mbits/sec
[ 5] 10.00-10.05  sec 553 KBytes 96.7 Mbits/sec
-----
[ ID] Interval      Transfer    Bandwidth
[ 5] 0.00-10.05   sec 0.00 Bytes 0.00 bits/sec
[ 5] 0.00-10.05   sec 128 MBytes 107 Mbits/sec
-----
sender
receiver

```

**Figure 16.** The test result of communication speed test 2.

In this study, the standard Ethernet communication speed of 100 Mbps was set as the target communication speed between the USVs. The obtained results confirmed that the communication speed between the leader USV and the follower USV was 107 Mbps, which satisfied the communication speed set as the target in this study.

#### 5.1.2. GNSS Performance Test

Among the sensors installed in the USV, the most important for navigation is the GNSS. It provides the variable values necessary for the calculation to control each USV, such as the current position, target position, current direction angle, target azimuth, and distance error, and simultaneously creates the target virtual point necessary for maintaining the swarm formation. Therefore, determining whether the sensor data outputted from the GNSS are reliable is crucial. Hence, in this study, two cases were considered to verify the performance of the GNSS:

1. Static performance testing; and
2. Dynamic state performance testing.

The static performance test was conducted at the U-Busan-14 point of the unified reference coordinates announced by the Korea Geographical Information Service. The experiment was conducted by placing one USV at a point 6.5 m north of the integrated reference coordinates and the other at a point 3.2 m west of the integrated reference coordinates to acquire data. At this time, the data output period of the GNSS was 10 Hz, and the data were acquired for 1 h. Figure 17 depicts the experimental process, and Figure 18 shows the experimental results.



**Figure 17.** Photo of the static state performance test.

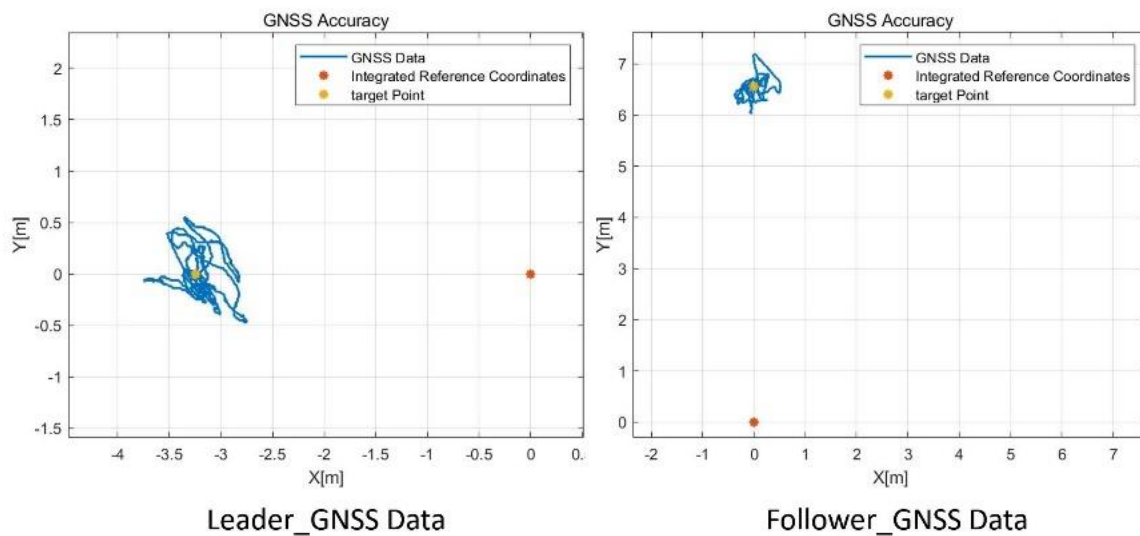


**Figure 18.** Results of the static state position data performance test.

As shown in the results, the average value of each GNSS position output almost coincides with the target coordinate, and the position error occurring during the test had a value within about  $\pm 0.5$  m. Therefore, in the static state, it is confirmed that the position data outputted from the GNSS are reliable.

The GNSS installed in each USV outputs not only the position data but also the heading data, and the heading data are essential to control the target heading of each USV. Therefore, the precision of the direction angle data outputted from the GNSS was confirmed. The experiment was conducted simultaneously in the same place as the static state performance test. Furthermore, it was arranged to face the true north ( $0^\circ$ ) direction indicated in U-Busan-14 to acquire data for 1 h and analyze the acquired data. The test results are shown in Figure 19.

An error of  $\pm 0.55^\circ$  occurred in the case of the sensor mounted on the leader USV based on true north ( $0^\circ$ ), and an error of  $\pm 0.76^\circ$  occurred in the case of the follower USV. Therefore, through the static state performance test, it is confirmed that the GNSS mounted on the USV has almost no performance difference between each sensor in the static state and that it outputs sufficiently reliable data.

GNSS data generate more errors in the dynamic state than in the static state [26]. Therefore, even if the static state of the GNSS installed in the USV is reliable, the dynamic state reliability should also be verified. Dynamic state performance tests were conducted on land.

Before proceeding with the test, the position data were acquired at each corner of a playground for 30 min, and the obtained values were averaged. The coordinates of each point (Table 3) were set to these average values.

After this calibration, the GNSS was moved from point 1 to point 4, and the test was carried out by acquiring and analyzing the position data and direction angle data outputted from the sensor. Figure 20 shows a conceptual diagram of the dynamic state test, and Figure 21 shows the position data results of the dynamic state test.

The results confirmed that the path to each point appeared in an almost perfectly straight line. Figure 22 shows the direction angle results of the dynamic state test.

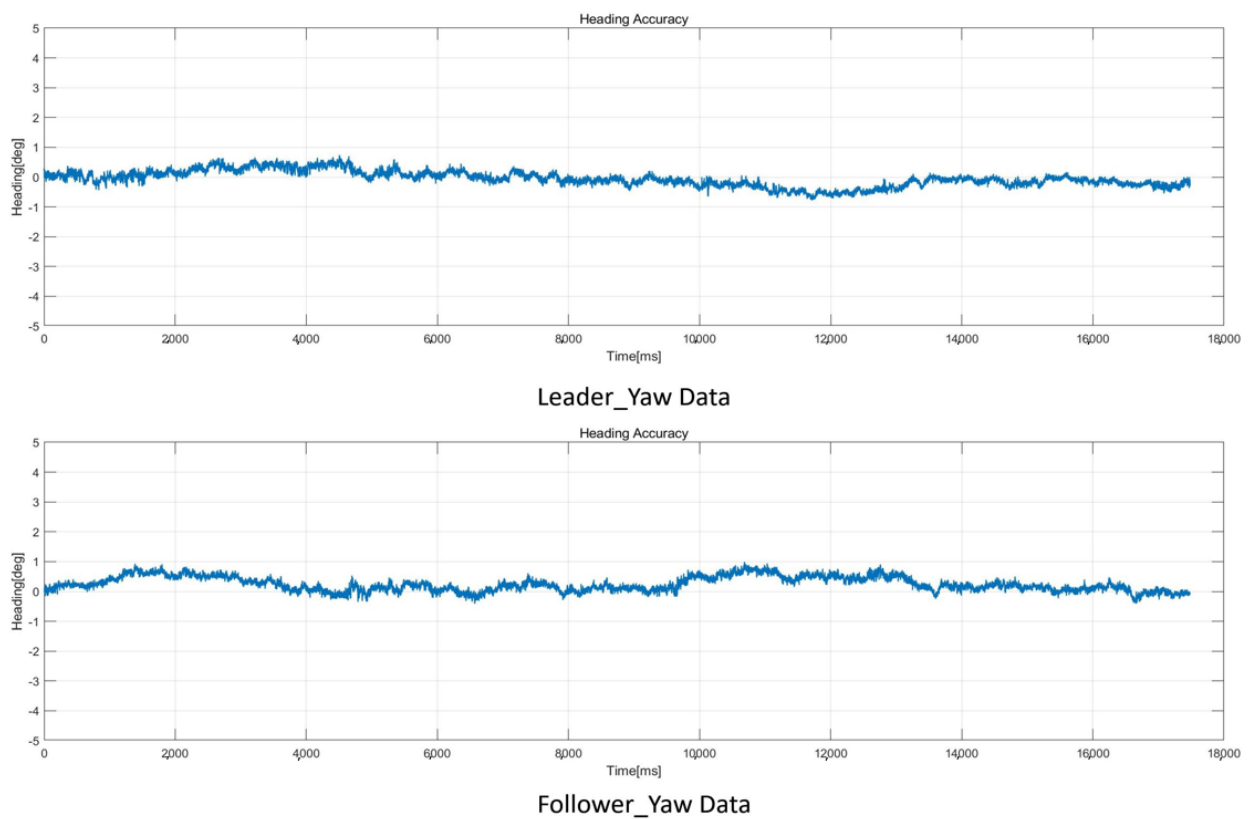


**Figure 19.** Results of the static state yaw data performance test.

**Table 3.** Test point coordinates.

	Latitude	Longitude
Point 1	35.0739915	129.0875807
Point 2	35.0741897	129.0880333
Point 3	35.0737509	129.0883212
Point 4	35.0735461	129.0878727

As a result, it was confirmed that the created pattern had a constant direction angle for each point through both rotations of each point. Therefore, it was confirmed through the test that the data of the GNSS were reliable even in the dynamic state.

### 5.2. USV Swarm Control Performance Test

In the swarm control performance test, after placing the leader and follower USVs at an arbitrary location, four waypoints were entered in the USV to drive it. After the driving was completed, by analyzing the acquired data, the test was carried out to confirm whether the leader and follower USVs maintained the swarm formation well. At this time, the swarm formation was set to the right side where the follower USV took a position on the right side of the leader USV. The leader and follower USVs were set to create a formation with an interval of 4 m. Table 4 lists the waypoint coordinates entered into the USV, and Figure 23 depicts a conceptual diagram of the cluster control performance test.



Figure 20. Diagram of the dynamic state performance test.

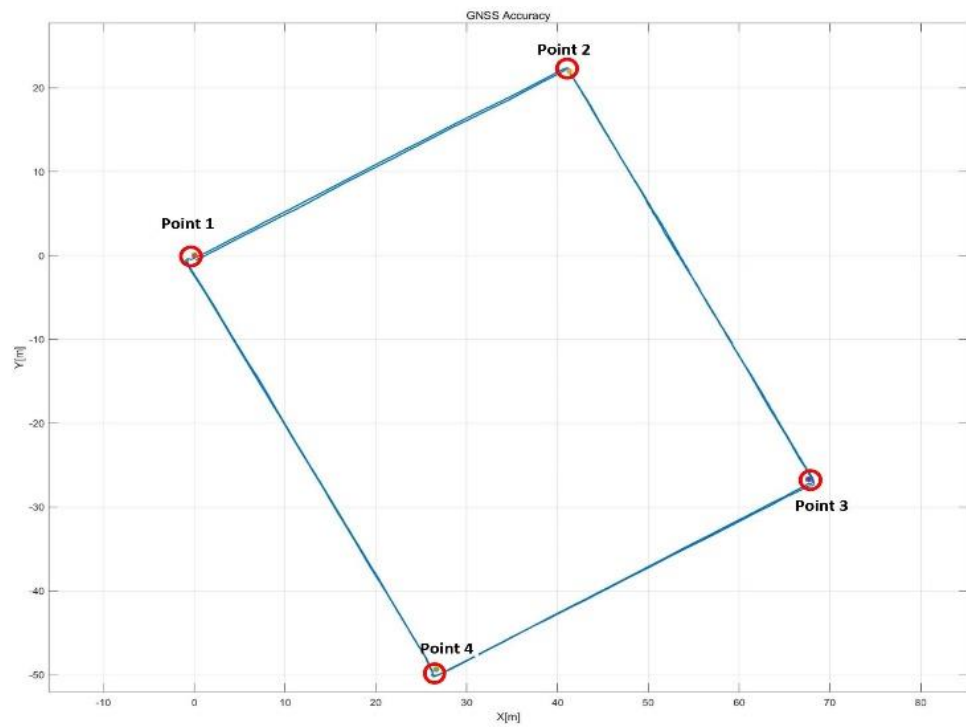


Figure 21. Results of the dynamic state test position data.

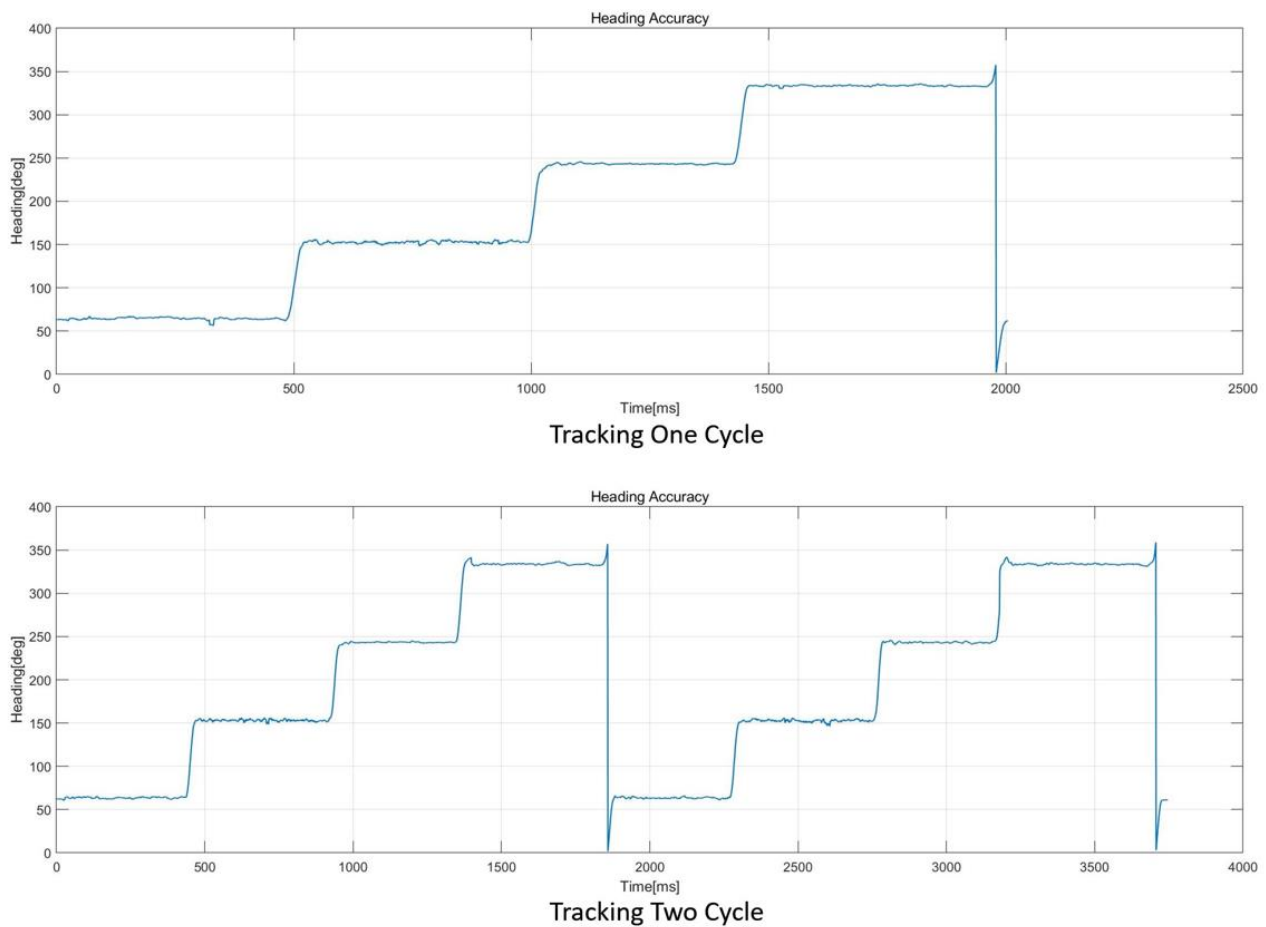


Figure 22. Results of the dynamic state test heading data.

Table 4. Waypoint coordinates.

	Latitude	Longitude
Point 1	35.0749359	129.0842590
Point 2	35.0746651	129.0848846
Point 3	35.0750885	129.0851746
Point 4	35.0753899	129.0846252

Among the swarm control performance test results, the tracking results are shown in Figure 24.

The results show that the follower USV, to the upper right corner of the leader USV, turns wide, and it can be confirmed that the leader USV and each point are driven maintaining a certain distance. The driving path of each USV operating from waypoint 3 to waypoint 4 deviated from the target driving path. The swarm formation that the leader and follower USVs aimed to maintain was well preserved even in situations where a path error occurred.

Figure 25 shows the direction angle results from the swarm control performance test results.

As shown Figure 25, the heading data of each USV showed a similar pattern, confirming that the vehicle was driven. This indicates that each USV maintained the swarm formation well. As can be observed, the slope of the direction angle data change in the follower USV (red) is gentler than that of the leader USV (blue) at each point. This pattern appears because the set swarm formation is the right side, where the follower USV is

located on the right side of the leader USV. Therefore, the rotation radius of the follower USV is larger than that of the leader USV.

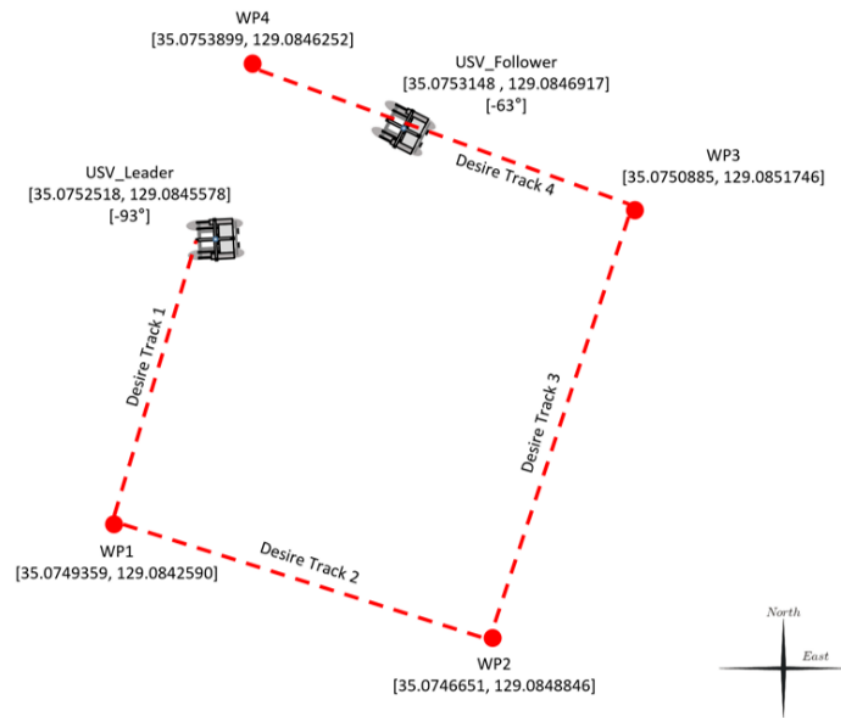


Figure 23. Diagram of the swarm control performance test.

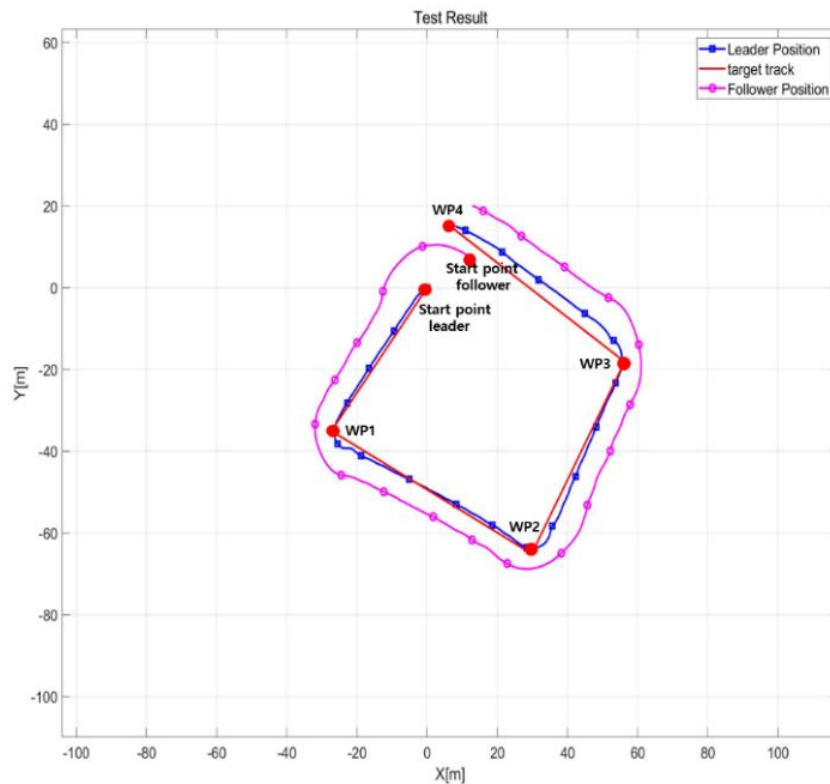


Figure 24. Tracking results of the swarm control performance test.

Figure 26 shows the distance data between the leader and follower USVs.

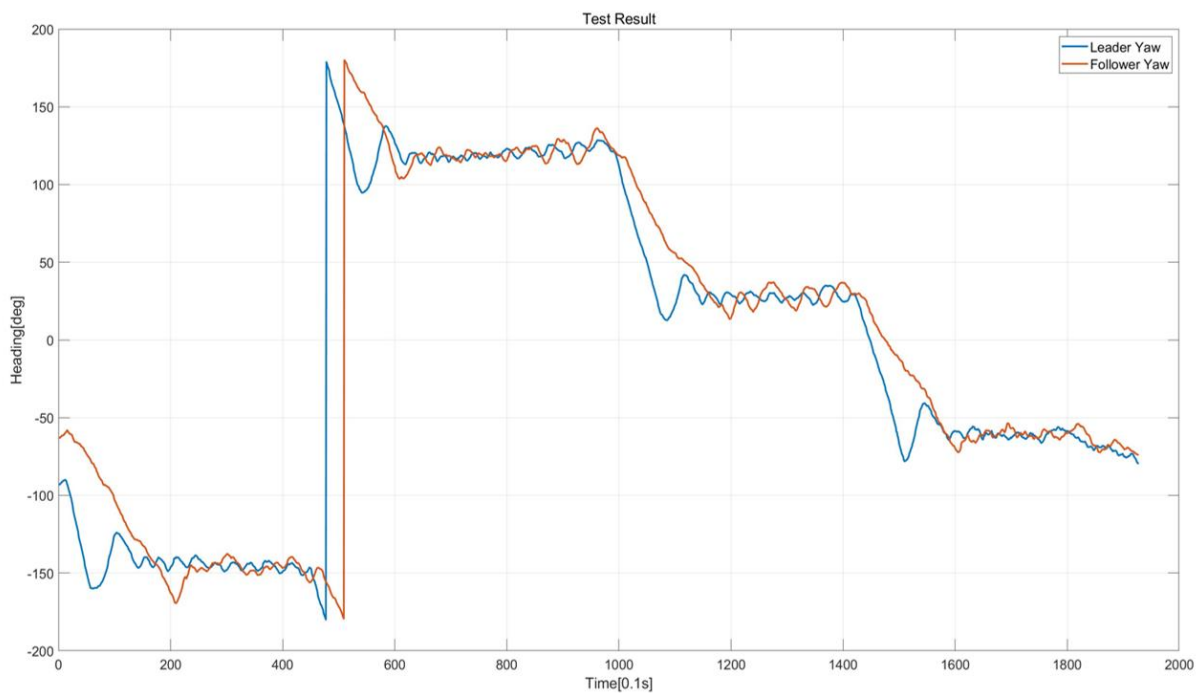


Figure 25. Heading results of the swarm control performance test.

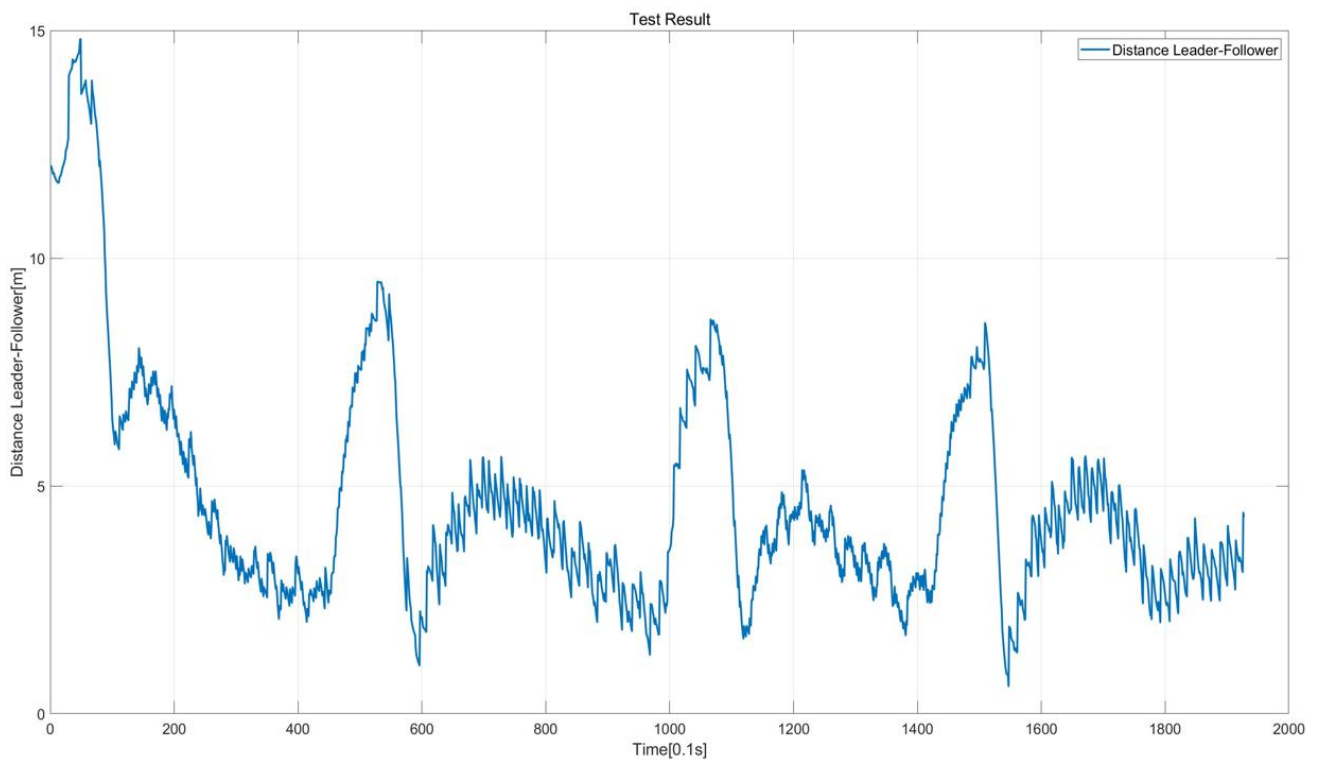


Figure 26. Distance results of the swarm control performance test.

At first, the leader USV and the follower USV, which initially had a distance of about 12 m, maintained a distance of 3–5 m over time. After turning at each WP point, the distance became more than 10 m. However, it is confirmed that the vehicle was driven while maintaining a distance of 3–5 m again after each turning motion was completed.

## 6. Conclusions

In this study, the leader–follower swarm control algorithm was explored to overcome the limitations of the single-individual USV system. A USV was developed to verify the performance in a real sea area using the leader–follower swarm control algorithm proposed in this study. The power and communication systems were designed to realize the target operation performance. In particular, in the power system, in preparation for an unexpected accident, a coulometer indicator was installed to monitor the battery status and to cut off the power in the case of an abnormality to increase safety. The communication system adopted the decentralization method and was designed in such a way that the land operation console, leader USV, and follower USV share each other’s data in real time to facilitate data sharing. As a result, a system that does not require fixed server facilities was developed. To enable smooth navigation in the marine environment, which is an environment with many disturbances, a CTE compensation algorithm was installed in the USV in addition to the basic navigation algorithm. The controller was designed so that a desired swarm formation can be realized using the swarm control algorithm built separately for each USV.

Before testing in an actual sea area, individual performance tests of each sensor were conducted to verify the data reliability of the sensors mounted on the USV. Through the actual sea area test, the performance of the swarm control algorithm, swarm formation controller, and navigation algorithm proposed in this study was verified. As a result, it was confirmed that the leader and follower USVs created the desired formation and followed the target trajectory.

In future research, it is necessary to compare the performance of the navigation algorithms (CTE compensation algorithm and swarm control algorithm) proposed in this paper and commonly used navigation algorithms, and research is needed to overcome the disadvantages of the leader–follower swarm control algorithm.

**Author Contributions:** J.-H.L., contributed to conceptualization, methodology, and writing—original draft preparation. S.-K.J. and H.-S.C., reviewed the correction and formula of the paper. D.-H.J. and H.-Y.P., analyzed the data in the paper. D.-Y.K. and K.-B.C., helped create illustrations for the paper. D.-W.J. and M.-J.K., helped create the platform used in the paper. M.-H.O., helped finance the research. All authors have read and agreed to the published version of the manuscript.

**Funding:** This research was a part of the project titled ‘Development of smart maintenance monitoring techniques to prepare for disaster and deterioration of port infra structures’, funded by the Ministry of Oceans and Fisheries, Korea, Fund number: 20210659.

**Institutional Review Board Statement:** Not applicable.

**Informed Consent Statement:** Not applicable.

**Data Availability Statement:** Data sharing not applicable.

**Acknowledgments:** The authors would like to thank all the peer reviewers for their valuable contributions to this paper.

**Conflicts of Interest:** The authors declare no conflict of interest.

## References

1. Cha, H.J. BT News (Marine Bio Materials Research Center). *Korean Soc. Biotechnol. Bioeng.* **2017**, *24*, 64–68.
2. Bentley, R.W. Global oil & gas depletion: An overview. *Energy Policy* **2002**, *30*, 189–205.
3. Nicholson, J.W.; Healey, A.J. The present state of autonomous underwater vehicle (AUV) applications and technologies. *Mar. Technol. Soc. J.* **2008**, *42*, 44–51. [[CrossRef](#)]
4. Kim, T.S.; Kim, C.H.; Lee, M.K. Study on the design and the control of an underwater construction robot for port construction. *Korean Inst. Navig. Port Res.* **2015**, *39*, 253–260. [[CrossRef](#)]
5. Chen, Y.; Liu, T.; Meng, S.Y.; Zhuang, Y. System modeling and simulation of an unmanned aerial underwater vehicle. *J. Mar. Sci.* **2019**, *7*, 444. [[CrossRef](#)]
6. Rodriguez, J.; Castaneda, H.; Gordilo, J.L. Design of an adaptive sliding mode control for a micro-AUV subject to water currents and parametric uncertainties. *J. Mar. Sci.* **2019**, *7*, 445. [[CrossRef](#)]

7. Cruz, D.; McClintock, J.; Perteet, B.; Orqueda, A.A.O.; Cao, Y.; Fierro, R. Decentralized cooperative control—A multivehicle platform for research in networked embedded systems. *IEEE Control Syst. Mag.* **2007**, *27*, 58–78.
8. Feddema, J.T.; Lewis, C.; Schoenwald, D.A. Decentralized control of cooperative robotic vehicles: Theory and application. *IEEE Trans. Robot. Autom.* **2002**, *18*, 852–864. [[CrossRef](#)]
9. Gu, Y.; Seanor, B.; Campa, G.; Napolitano, M.R.; Rowe, L.; Gururajan, S.; Wan, S. Design and flight testing evaluation of formation control laws. *IEEE Trans. Control Syst. Technol.* **2006**, *14*, 1105–1112. [[CrossRef](#)]
10. Sallama, A.; Abbod, M.; Khan, S.M. Applying Sequential Particle Swarm Optimization Algorithm to Improve Power Generation Quality. *Int. J. Eng. Technol. Innov.* **2014**, *4*, 223–233.
11. Lee, K.R. Design of Decentralized Behavior-Based Network for the Formation Control and the Obstacle Avoidance of Multiple Robots. Ph.D. Thesis, Ajou University, Gyeonggi-do, Suwon-si, Republic of Korea, 2018.
12. Park, S.B.; Park, J.H. A Study on Formation Control Algorithms of Multi-Obstacles Collision Avoidance for Autonomous Navigation of Swarm Marine Unmanned Moving Vehicles. *J. KNST* **2020**, *3*, 56–61. [[CrossRef](#)]
13. Lee, S.J.; Hong, S.K. Leader Robot Controller Considering Follower with Input Constraint. *Trans. Korean Inst. Electr. Eng.* **2012**, *61*, 1032–1040. [[CrossRef](#)]
14. Tak, M.H.; Kim, J.S.; Joo, Y.H.; Ji, S.H. Formation Control for the Obstacle Avoidance of Swarm Robots based Leader-Follower Robots. *Korean Inst. Electr. Eng.* **2013**, *10*, 171–172.
15. Julio, G.G.; Daniel, P.A.; Enrique, C.; Cristina, C. Unsupervised Adaptive Multi-Object Tracking-by-Clustering Algorithm with a Bio-Inspired System. *IEEE Access* **2022**, *10*, 24895–24908.
16. Fossen, T.I. *Guidance and Control of Ocean Vehicles*; John Wiley & Sons: Hoboken, NJ, USA, 1994.
17. Fossen, T.I. *Handbook of Marine Craft Hydrodynamics and Motion Control*; John Wiley & Sons: Hoboken, NJ, USA, 2011.
18. Cho, H.J.; Jeong, S.K.; Ji, D.H.; Tran, N.H.; Vu, M.; Choi, H.S. Study on control system of integrated unmanned surface vehicle and underwater vehicle. *Sensors* **2020**, *20*, 2633. [[CrossRef](#)] [[PubMed](#)]
19. Lee, J.H.; Jin, H.S.; Cho, H.J.; Jiafeng, H.; Jeong, S.K.; Ji, D.H.; Choi, H.S. A New Complex Marine Unmanned Platform and Field Test. *J. Mar. Sci. Technol.* **2020**, *28*, 538–547.
20. Lee, S.J. Leader Robot Controller Considering Follower with Input Constraint. Master's Thesis, Ajou University, Suwon-si, Republic of Korea, 2012.
21. Dierks, T.; Jagannathan, S. Control of nonholonomic mobile robot formation: Back stepping kinematics into dynamics. In Proceedings of the IEEE Multi-Conference System Control, Suntec City, Singapore, 1–3 October 2007.
22. Kanayama, Y.; Kimura, Y.; Miyazaki, F.; Noguchi, T. A stable tracking control method for an autonomous mobile robot. In Proceedings of the IEEE International Conference Robotics and Automation, Cincinnati, OH, USA, 13–18 May 1990.
23. Consolini, L.; Morbide, F.; Prattichizzo, D.; Tosques, M. Leader-follower formation control of nonholonomic mobile robots with input constraints. *Automatica* **2008**, *44*, 1343–1349. [[CrossRef](#)]
24. Choi, I.S. Range Finder based Leader-Follower Formation Control of Multiple Mobile Robot in Outdoor Environments. Master's Thesis, Korea University, Seoul, Republic of Korea, 2013.
25. Cho, H.J. A Study on Control System of Wire Integrated Unmanned Surface Vehicle and Unmanned Underwater Vehicle. Master's Thesis, Korea Maritime & Ocean University, Busan, Republic of Korea, 2020.
26. Tadashi, T.; Omine, M.; Itani, K.; Ehsani, R. Evaluation of the Dynamic Accuracy of a GPS Receiver: Is dynamic accuracy the same as static accuracy? *Eng. Agric. Environ. Food* **2011**, *4*, 54–61.

**Disclaimer/Publisher's Note:** The statements, opinions and data contained in all publications are solely those of the individual author(s) and contributor(s) and not of MDPI and/or the editor(s). MDPI and/or the editor(s) disclaim responsibility for any injury to people or property resulting from any ideas, methods, instructions or products referred to in the content.